공학석사 학위논문

Study on Thermal Management of Power Electronics System for Electric Vehicles using Two-phase Cooling

비등냉각을 이용한 전기자동차용 전력전자시스템의 열 관리에 대한 연구

2020 년 8 월

서울대학교 대학원

기계공학부

엄 준 영

Abstract

Study on Thermal Management of Power Electronics System for Electric Vehicles using Two-phase Cooling

Jun Young Eom
Mechanical Engineering
The Graduate School
Seoul National University

The necessity of both higher power density and miniaturization of power electronics is on the rise, and accordingly, thermal management of it becomes an important issue with the expansion of the electric vehicle industry. Boiling heat transfer has a higher heat transfer coefficient than normal single-phase heat transfer, and the cooling system has excellent cooling performance because it absorbs most of the heat as the phase change energy of the working fluid. As the power electronics require still more electrical energy transfer, it is expected

that conventional water-cooled system will reach limit of its thermal management in lowering the peak temperature and maintaining uniform temperature distribution in the electric device at the same time.

In order to overcome these difficulties, two-phase cooling system with pin-fin type heat sink using refrigerant as a working fluid is proposed instead of the conventional single-phase water-cooled system. By removing high heat flux through two-phase cooling, it is possible to maintain a uniform device temperature within the temperature range allowed for the device even at high power level conditions. In particular, many studies have been conducted using dielectric liquid as a working fluid to apply a boiling heat transfer cooling system to the electric and electronic fields. In this study, Infinion's IGBT module (inverter) for hybrid electric vehicle (HEV) with pin-fin type heat sink was adopted as an experimental apparatus, and HFE-7100 which boils under operating condition of the power electronics was selected as a refrigerant.

In order to calculate the amount of heat generation for the power electronics, electric power transfer and loss model was developed for the light-duty electric vehicle. As result of the simulation, the power loss was implemented through the heater attached to the power electronics module with heat sink. The experiment was conducted by changing the working fluid, water and HFE-7100, and the temperature and distribution of it were compared. The

experimental results show that two-phase cooling system using the refrigerant showed lower peak temperature with reasonable uniformity, which indicates that the life and reliability of the device would be improved.

Key words: Electric vehicle, Power electronics system, Two-phase cooling, Pin-fin type heat sink, Thermal management, HFE-7100

Student Identification Number: 2018-27952

Contents

List of Tables

List of Figures

Nomenclatures

A	Area (m^2)
F	Force (N)
I	Current (A)
L	Inductance (H)
P	Power (W)
Q	Heat (W)
T	Temperature (°C)
T	Torque (N·m)
t	Time (s)
v	velocity (m/s)
V	Voltage (V)
w	Angular speed (rad/s)
λ_f	Flux linkage (wb)
Φ	Phase (°)

Subscript

cond	Conduction loss
sw	Switching loss
acc	Accleration
fric	Friction
grad	Gradient
air	Air resistance
drv	driving
c	Collector
e	Emitter
d	d-axis
q	q-axis
u	u-phase
v	v-phase
w	w-phase
s	Saturation
r	Reverse recovery

Chapter 1. Introduction

1.1 Background of the study

The amount of carbon dioxide and greenhouse gases emitted by fossil fuels is increasing rapidly every year. Not only that, but the price of CER (Certified emission reduction) has increased 1.77 times compared to 2018. As the price of CER rises day by day, concern of many companies is increasing, and the reduction of carbon dioxide emissions is expected to have a significant impact on national economy. Since around 28% of carbon dioxide emissions are generated by transportation, reducing carbon dioxide emissions in the transportation sector is still a major issue worldwide. So, many countries around the world encourage to use hybrid and electric vehicles (HEV/EV) as one of the solutions to reduce carbon dioxide emissions. HEV / EV is recognized as an environmentally friendly product by academia in terms of carbon dioxide emissions because it can use electricity produced from eco-friendly and renewable energy sources such as wind, hydro, and solar powers and can actually help reduce carbon dioxide emissions. As electric vehicles emerged as an alternative to gasoline and diesel vehicles, research on power electronics system is becoming more active. In particular, research and development on the power electronics system is actively carried out. Power electronics system, which are called power trains of electric vehicles, are largely composed of batteries, inverters, and motors.

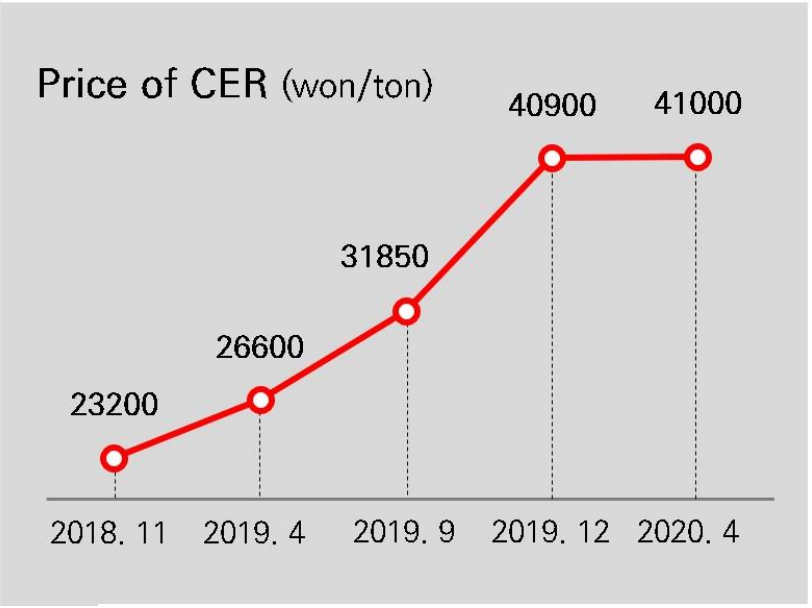

Fig. 1.1 Price of certified emission reduction [1]

In power electronics system, the electrical energy stored in the batteries is transferred to the inverter in the form of DC, and the inverter converts single-phase DC type electrical energy into 3-phase AC. Electric vehicle motors currently have power capacities from 80 kW to 120 kW, and are expected to increasing further in the future. As a result, the size of the electric energy that the IGBT (Insulated gate bipolar transistor), which is a core part of the inverter, needs to convert is also increasing, but due to the inefficiency in the energy conversion process, the IGBT module generates a lot of heat. It is really important to properly cool the heat generated by the IGBT module, even in order to increase the overall stability of the power electronics system and the life, stability and conversion efficiency of the IGBT module. In this regard, research on miniaturization and energy density increase of IGBT, which is a key component of electric vehicles, has been actively conducted. As the power rating of the motor for electric vehicle increases, the size of the heat sink for cooling the heat generated by the IGBT module must also increase, but due to the limitations of the space inside the vehicle, the ultimate solution is to improve the cooling efficiency of the IGBT module. For example, Meysenc et al [2] increase the cooling capacity of IGBT inverter module from 50 W/cm² (typical for an air-cooled heat sink) to 120 W/cm² (typical for liquid-cooled cold plate) and it makes possible to double the output current of the inverter from 40 A/cm² to 80 A/cm². Therefore, thermal management solution for efficiently managing the heat generated by the IGBT module is important and this research presents a method that can be an effective solution.

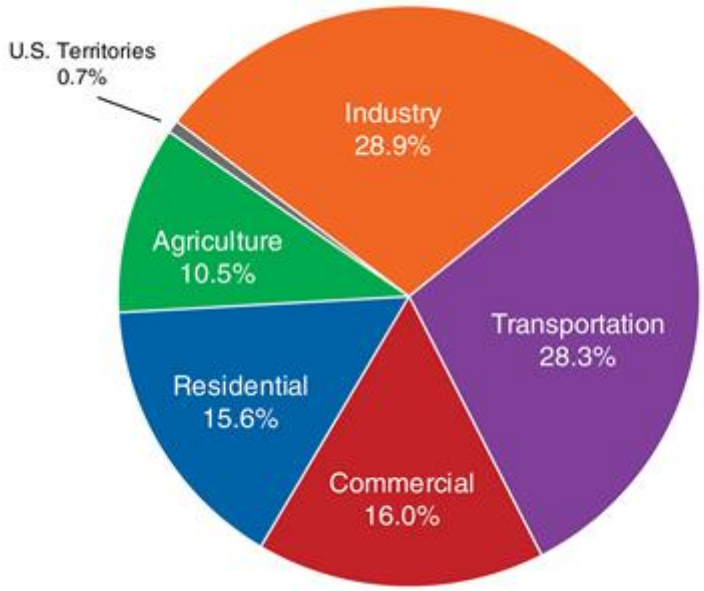

Fig. 1.2 US greenhouse gas emissions by economic sector, 2018 [3]

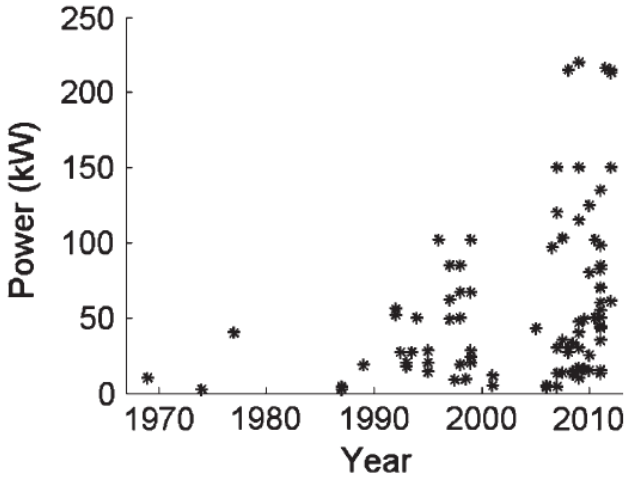

Fig. 1.3 Power rating of EVs motor released on the market [4]

1.2 Literature survey

1.2.1 Jet impingement and spray cooling method

Jet impingement cooling is a method of shooting liquid jet on the surface of the base plate in order to achieve not only high heat transfer coefficients but also very low thermal resistances. Spray cooling method is technology which can be applied to high heat flux applications. It utilizes both liquid phase and liquid-vapor phase. Combination of several mechanisms, which are forced convection, and impinging spray droplets, and boiling of the liquid on the sprayed surface, makes high heat transfer performance.

Recently, various studies of cooling method including jet impingement and spray cooling have been conducted for thermal management of power electronics for increasing heat transfer coefficient and reducing thermal resistance. For example, Matthew et al. [5] conducted experimental studies and simulations of cross-shaped jet impingement heat transfer using Hfe-7100 and showed that the cross-shaped jet also results in local heat transfer coefficients that exceed the stagnation point value of the circular jet. Bhunia at al. [6-7] investigated an open and closed loop liquid micro-jet array and spray impingement boiling at normal and reduced pressure. They have been shown to enhance the module output power rating by 30% and 80%, respectively, in comparison to conventional air-cooling technology. Parida et al. [8] supposed various cooling options based on jet impingement for high performance micro scale electronic systems. Simulations about direct liquid jet impingement was

validated by theory and experiments. They illustrated that significant improvements of thermal performance and volume reduction was shown both experimentally and numerically.

Mudawar et al. [9] studied spray cooling using a dielectric liquid, HFE-7100, which can be directly sprayed onto power electronics chips. They showed systematic methodology for predicting the cooling performance of pressure spray nozzles and also validated the performance of HFE-7100 experimentally for different flow rates, subcooling and pressures maintaining surface temperatures safely below 125°C. Bostanci et al. [10] conducted 2000 h of test under constant heat flux of 200 W/cm² using spray cooling system simulated by DBC board. They concluded that spray cooling offers the possibility to run the inverter module at higher current density with fewer and smaller devices, resulting in significant potential cost savings and long-term reliability. Rowden et al. [11] designed and tested a spray cooling system having large and double-sided area and showed that using a dielectric fluid FC-72, spray cooling system can remove heat fluxes up to 50 W/cm² in case of relatively large areas.

1.2.2 Two-phase cooling method for IGBT module

Two-phase cooling method utilizes the latent heat absorbed during evaporation of the working fluid and through this method, high heat transfer coefficient and temperature uniformity in applications of high heat flux can be achieved. Mudawar et al. [12-13] designed an R134a-cooled two-phase micro-channel heat sink which is capable of providing a heat transfer coefficient up to

50,000 W/m²K. They conducted experimental study about pressure drop characteristics and heat transfer characteristics of parallel rectangular micro-channels. P. Wang et al. [14] conducted simulation study about cold-plate device-level analysis and motor inverter system-level evaluation of two-phase cooling for thermal management of high-power electronics using the Toyota Prius motor inverter as the test vehicle. They used R134a as a working fluid and showed that R134a two-phase cooling have much better cooling performance at lower energy consumption and lower flow rate. With an R134a-cooled two-phase cold plate, the maximum IGBT temperature was lower and temperature distribution was more uniform than ethylene glycol/water cooled single-phase cold plate. Qian et al. [15] reviewed and analyzed researches of thermal management of IGBT and classified into different categories such as analytical models, numerical models and thermal network models. Also, they showed and categorized various cooling method of IGBT such as two-phase cooling, spray cooling, jet impingement cooling, etc.

1.3 Objective and scope

As the power consumption of electronic devices increases, the amount of heat generation also increases. Therefore, many methods of effectively removing heat generated from electronic equipment has been proposed. In this paper, two-phase cooling method is proposed as one method of removing heat from electronic devices in electric vehicles.

In chapter 2, the introduction of inverter module for electric vehicle used in the experiment and the process of creating a numerical model for calculating the heat generation of the inverter are covered. The conduction loss and switching loss occurring in the power semiconductor were explained. Also, using the automotive dynamics and various methods of controlling the current input to the induction motor, the heat generation of the inverter was obtained according to the driving method by comparing the heat generation of the inverter with actual driving experiment data.

In chapter 3, two-phase cooling method using refrigerant is suggested as a method to compensate for the limitations of the existing water cooling, for example, low temperature uniformity and high peak temperature. HFE-7100 was selected as the working fluid to be used for boiling cooling because it can boil well in the temperature range inside the vehicle and requires low electrical conductivity to cool the electric device. By applying two-phase cooling, it was found through experiments that the operating temperature of the inverter was lowered and the temperature inside the inverter became more uniform than the conventional water single-cooling method.

Chapter 2. Numerical model for predicting heat generation of inverter module.

2.1 Losses of power semiconductor

As shown in the figure 2.1, the inverter installed in the electric vehicle is a device for driving motor, and it converts the direct current power of the battery into three-phase alternating current power and transfer to the motor. The core part of the inverter is a semiconductor called IGBT (Insulated gate Bipolar transistor), and energy losses in IGBT divided into conduction loss and switching loss. Conduction losses are the losses that occur when IGBT is on-state, and are expressed as the product of on-state collector-emitter voltage (V_{ce_sat}) and on-state collector current (I_c) which is caused by internal resistance. The average power dissipated by conduction loss is given by equation as follow.

$$P_{cond} = \frac{1}{t_p}\int_0^{t_{cond}} I_c(t)V_{ce}(t)\,dt \tag{2.1}$$

The inverter converts DC power into three-phase AC power through PWM method. And the 6 IGBTs inside the inverter switch at a speed of about 8000hz during the process of power conversion and switching loss is generated. Switching loss occurs because transistor current and voltage cannot abruptly change during switching process. For example, as soon as IGBT becomes

turned on, the collector-emitter voltage drops rapidly and the collector current increases rapidly. During the transition interval, both the current and voltage through the semiconductor are substantially greater than zero which lead to large power loss. Switching losses depend on V_{ce}, I_c, switching frequency and the average power dissipated by switching loss is given by Equation as follow.

$$P_{sw} = \frac{1}{t_p}\left(\int_0^{t_r} I_{c\_r}(t)V_{ce\_r}(t)\,dt + \int_0^{t_f} I_{c\_f}(t)V_{ce\_f}(t)\,dt\right) \quad (2.2)$$

As a result, total losses of IGBT can be expressed in the following equation.

$$P_{IGBT} = P_{cond} + P_{sw} \quad (2.3)$$

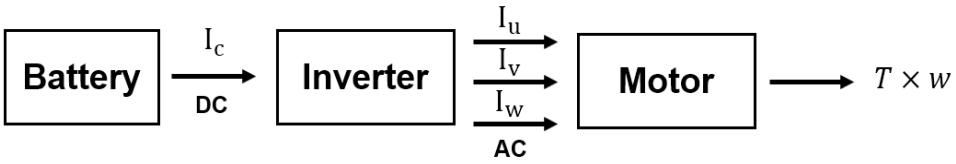

Fig. 2.1 Energy flow in the power electronics system

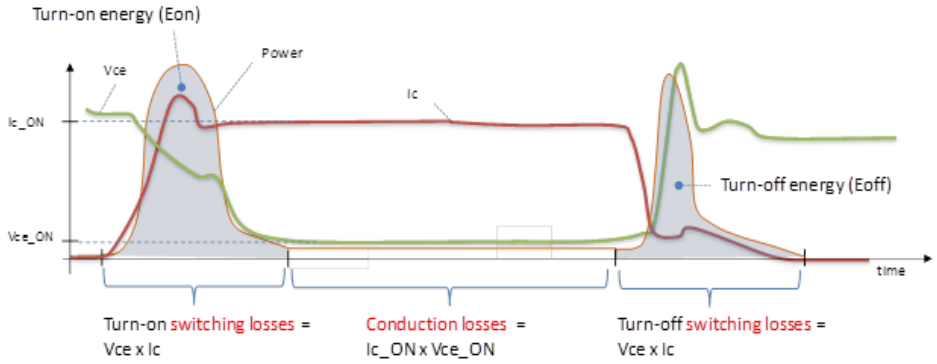

Fig. 2.2 Losses of power semiconductor [45]

2.2 Numerical model

2.2.1 Purpose

A numerical model was created in order to predict the amount of heat generated in the inverter module and determine the ‘high heat flux range’. By applying external factors such as driving speed and slope of the road, and vehicle characteristics such as vehicle weight and air resistance, the amount of heat generated by the inverter under specific driving conditions was calculated. In particular, in order to calculate the maximum amount of heat that can be generated in the inverter, the heat generation was measured by applying extreme driving conditions, for example, a condition of driving a 30% slope at 200 km/h. Since the amount of heat generation is determined by the current input to the inverter, a study on the energy flow of the entire power electronics system was conducted to calculate the inverter input current. So, the inverter input current was obtained by inversely calculating the energy flow of the entire power electronic system. In particular, since the control method of the motor is changed according to the driving speed, the current amount according to this is also derived in a different way.

2.2.2 Automotive dynamics

The motor converts electrical energy to mechanical work, that is, torque and angular velocity, and these are is determined by the speed of the vehicle, slope

of the road, and other parameters such as weight and shape of the vehicle. We selected 'Nexo', a Fuel cell Electric vehicle of Hyundai motors, as a vehicle model and three driving conditions as described in the table 2.1. The torque and angular velocity required for each of the three driving conditions were calculated using the specifications of Nexo. Three driving cases were selected, and for each driving mode, the output torque and rotational speed of the motor were calculated through basic theory of automotive mechanics in consideration of things such as the weight, and other coefficients of the vehicle.

$$F_{drv} = F_{acc} + F_{fric} + F_{grad} + F_{air}$$
$$= Ma + \mu Mg\cos\theta + Mg\sin\theta + 0.5C_dA * 1.23{v_{car}}^2 \quad (2.4)$$

$$P_{drv} = F_{drv} \times v_{car} \quad (2.5)$$

$$v_{car} = r_{wheel} \times w_{wheel} \quad (2.6)$$

$$w_{motor} = \lambda w_{wheel} \quad (2.7)$$

2.2.3 Motor and inverter input current

IPMSM (Interior Permanent Magnet Synchronous Motor) is the most commonly used for electric vehicles. IPMSM is widely used in electric vehicles due to its high output torque and wide weak magnetic field driving range. In order for the motor to generate a specific torque and angular speed, a specific current combination is required, and the method of combining currents depends on the speed of the motor. In general, motor is controlled by MTPA (Maximum Torque per Ampere) control when the angular speed of the motor is low, and

Flux weakening control when high, and MTPV (Maximum Torque per Voltage) control when super-high. Since the driving conditions used in this simulation are the regions of the low speed and high speed, the current required by the motor was calculated using the MPTA control and Flux weakening control methods. In IPMSM torque is determined by the following equation.

$$T = \frac{3}{2}\frac{P}{2}\left(\lambda_f i_q + \left(L_d - L_q\right) i_d i_q\right) \tag{2.8}$$

P is pole number, L_d, L_q are inductance of d-axis and q-axis each and λ_f is Magnetic flux interlinkage. Since P, L_d, L_q and λ_f are unique parameter of the motor, torque can be calculated by determining i_d and i_q. IPMSM use two kinds of method to determine i_d and i_q according to its angular velocity. The conditions for determining the operating area of the interior permanent magnet synchronous motor are generally determined by the maximum stator current $I_{s,max}$ and maximum DC voltage $V_{s,max}$ that can be applied to the motor. Therefore, as in equation 2.9, the vector sum of d-axis and q-axis currents in the synchronous coordinate system is limited to the magnitude of the stator maximum current. In addition, the voltage limit is determined according to the modulation method of the three-phase output voltage from the determined DC voltage level as in equation 2.10.

$$I_d^2 + I_q^2 = I_{s,max}^2 \tag{2.9}$$

$$V_d^2 + v_q^2 = V_{s,max}^2 \tag{2.10}$$

At low velocity, MTPA control is used, which select the d-axis and q-axis currents with the smallest stator current (I_s) among the combination of countless currents generating the same torque. In MTPA control, since the area of the voltage limiting ellipse is sufficiently large in the area where the rotational speed of the IPMSM is below the base speed, the voltage limiting condition is always satisfied, and only the current limiting condition acceptable for the motor needs to be satisfied as shown in the figure 2.3. Combining the equation 2.8 and differentiating equation of 2.9, we can obtain equations 2.11 and 2.12, which are current combination in the MTPA control.

$$\frac{\partial(I_d{}^2 + I_q{}^2)}{\partial I_d}\frac{\partial T}{\partial I_q} - \frac{\partial(I_d{}^2 + I_q{}^2)}{\partial I_q}\frac{\partial T}{\partial I_d} = 0 \tag{2.11}$$

$$I_d = \frac{-\lambda_f + \sqrt{\lambda_f{}^2 + 8(L_d - L_q)^2 I_s{}^2}}{4(L_d - L_q)} \tag{2.12}$$

As the rotational speed of the IPMSM increases, the size of the voltage limiting ellipse becomes smaller. Then the MTPA operating point meets the voltage limiting ellipse, from which point it will start flux weakening control. As the rotational speed of the OPMSM continues to increase, the voltage limiting ellipse is below the MTPA curve. Therefore, the position of the command current also moves along the current limit source to the d-axis and q-axis. It can be seen that the effective magnetic flux decreases because the d-axis current increases negatively. In the flux weakening control, the voltage conditions are expressed as equation 2.13 and 2.14. ($R_s I_d + L\frac{dI_d}{dt}$ and $R_s I_q +$

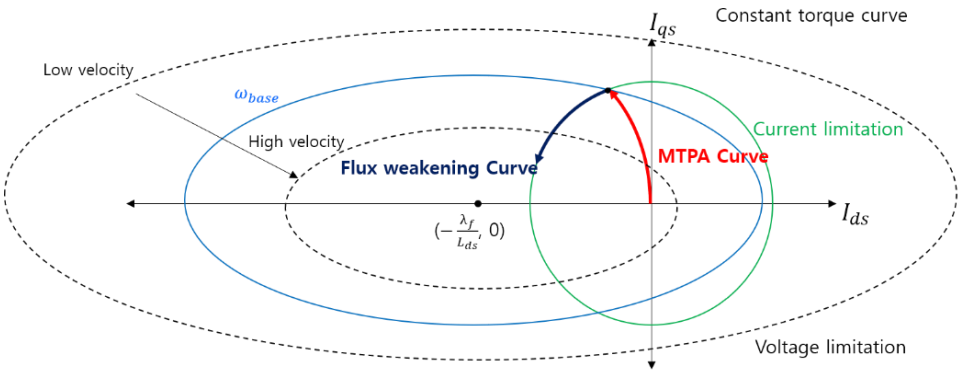

Fig. 2.3 Curves of MTPA control method and Flux weakening control method of IPMSM in I_d, I_q plane.

$L\frac{dI_q}{dt}$ terms are very small and may be omitted.)

$$V_d = \left(R_s I_d + L\frac{dI_d}{dt}\right) - \omega L_q I_q \approx -\omega L_q I_q \tag{2.13}$$

$$V_q = (R_s I_q + L\frac{dI_q}{dt}) + \omega L_d I_d + \omega\lambda_f \approx \omega L_d i_d + \omega\lambda_f \tag{2.14}$$

Combining Eqn. 10, 11, 13 and 14, d-axis and q-axis current in Flux weakening control can be calculated.

$$I_d = \frac{L_d\lambda_f - \sqrt{(L_d\lambda_f)^2 + (L_q^2 - L_d^2)\left\{\lambda_f^2 + (L_q I_s)^2 - (\frac{V_{s,max}}{w})^2\right\}}}{L_q^2 - L_d^2} \tag{2.15}$$

$$I_q = \sqrt{I_{s,max}^2 - {i_d}^2} \tag{2.16}$$

The motor input current was obtained by appropriately applying MTPA control and Flux weakening control for various driving conditions. In particular, the motor specification was applied to the simulation program 'Flux motor' to obtain a torque-current map as shown in figure 2.4, and the required torque previously calculated for each driving case, were applied to the map, and we derive the current combination for each case. Finally, motor input current and inverter input current I_c can be obtained as follows.

$$I_u = \sqrt{I_d^2 + I_q^2}\cos(wt + \phi),\ \phi = \tan^{-1}(I_q/I_d) \tag{2.17}$$

$$I_v = \sqrt{I_d^2 + I_q^2}\cos(wt + \phi - 120^o) \tag{2.18}$$

$$I_w = \sqrt{I_d^2 + I_q^2}\cos(wt + \phi + 120^o) \quad (2.19)$$

$$I_c = I_u + I_v + I_w \quad (2.20)$$

2.2.4 Total power loss of inverter

The amount of heat generated by an inverter for an electric vehicle is determined by the amount of current input to the inverter. In this study, the power loss data such as conduction losses and switching losses of IGBT and diode according to the inverter input current value can be obtained through 4 characteristic diagrams from datasheet of inverter module as shown in the figure 2.5 and 2.6. Collector-emitter voltage and switching loss values of IGBT and diode per pulse can be obtained by using the inverter input current (I_c) and IGBT junction temperature derived in the previous process through the characteristic diagram. Table 2.1 shows the total inverter input current, conduction loss, switching loss, and total heat dissipation values of each driving mode by comparing simulation results and driving experiment data from Hyundai motors. In the case of conduction loss and switching loss, it is the sum of the heating values of IGBT and diode each. In the case of inverter heat generation, it shows an error of less than 10%, which is judged to be a reliable simulation result.

Table 2.1 Driving mode (3 cases) and heat generation comparison calculated by simulation and actual driving experiment data from Hyundai motors.

Driving mode	Simulation results				Driving experiment data		Error
	I_c [A]	Q_{cond} [W]	Q_{sw} [W]	Q_{total} [W]	I_c [A]	Q_{total} [W]	
50km/h, 8%	175	319.6	295.6	615.2	173.7	563.8	9.12%
100km/h, 6%	165	297.9	283.9	581.9	168.1	542.8	7.20%
140km/h, 0%	183	337.4	305.2	642.6	167.3	590.3	8.86%

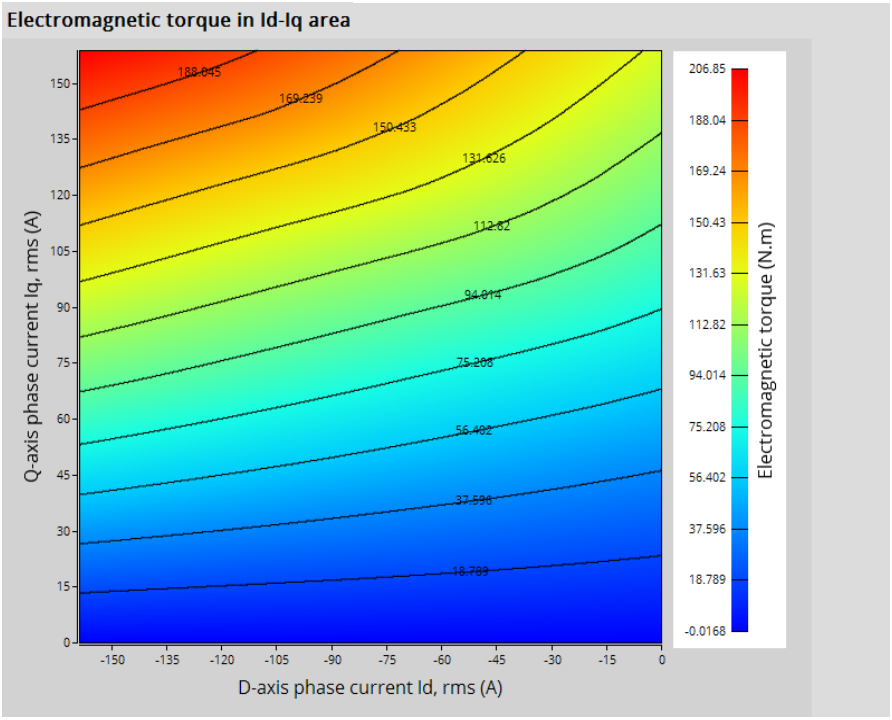

Fig 2.4 Torque-current map derived from simulation program 'Flux motor'

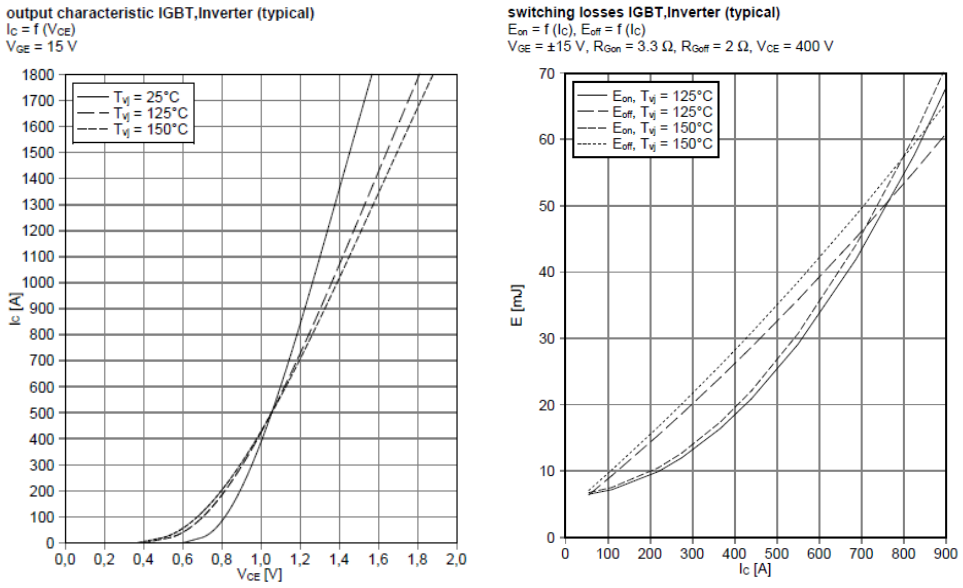

Fig 2.5 Losses characteristic of IGBT as a function of inverter input current

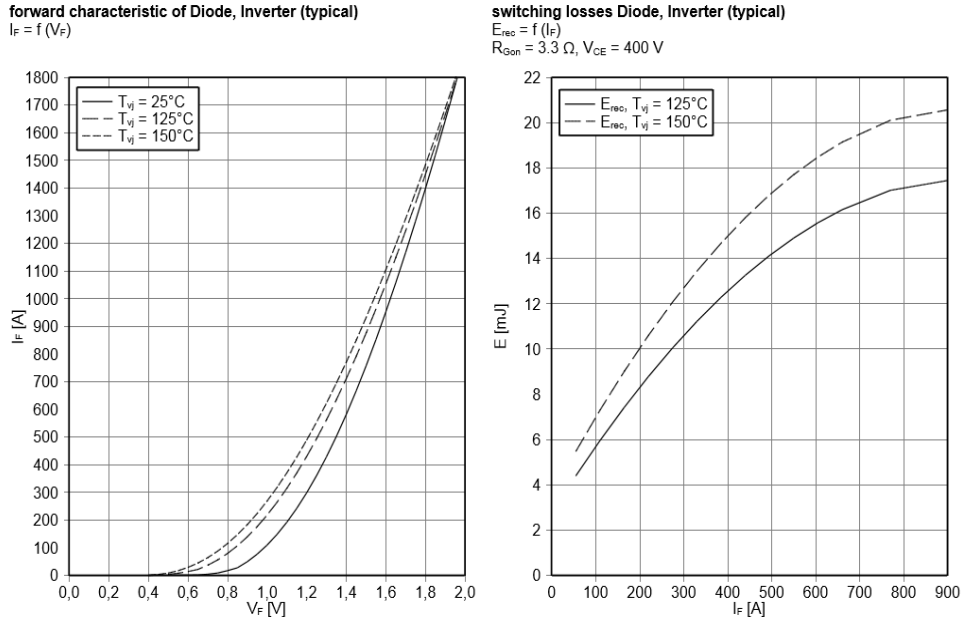

Fig 2.6 Losses characteristic of diode as a function of inverter input current

Chapter 3. Experimental results of water single-phase cooling and HFE-7100 two-phase cooling

3.1 Experimental setup

3.1.1 Experimental plans

In experiment, two-phase cooling using refrigerant HFE-7100 was proposed as a method of cooling the inverter. As experimental plan, the heat generation of the IGBT module obtained by using the numerical model was verified by referring to the literature on the cooling method of the inverter for electric vehicles which was more than 1.2 kW. In response to the increase in motor output due to the enlargement of the electric vehicle in the future and the increase in the heat generation of the inverter, the heat generation is assumed to be up to 2.0 kW, which was applied in the experiment. In order to generate heat of from 1.2 kW to 2.0 kW, a heating module was manufactured that mimics the amount of heat generated by the inverter was manufactured instead of operating the actual inverter. And water single-phase cooling and HFE-7100 two-phase cooling experiment are conducted and measure the temperature at six points inside the heating module. The temperature of each point was measured by measuring the temperature of two points of the brass heating element, and the

temperature of the IGBT surface was calculated by extrapolation. Inverter cooling experiments using water single-phase cooling and HFE-7100 two-phase cooling was conducted. The average value of the temperature at six points in each method was set as the operating temperature of the inverter, and the maximum temperature difference and the standard deviation of the temperature were calculated using the temperature distribution at the six points to compare the operation temperature and temperature uniformity of the inverter.

3.1.2 Heating module cooling system

The process of manufacturing the heating module is as follows. The inverter (Model: FS900R08A2P2_B31) constituting power electronics system of Hyundai Motors fuel cell electric vehicle 'NEXO' was selected as an experimental inverter. Since the inverter transmits three-phase alternative current power to the motor, it is divided into three areas. In each area, two IGBTs and diodes are placed in pairs, and each IGBT and diode is divided into four parts to prevent overcurrent as shown in the figure 3.1. the two IGBT-diode pairs in each area alternately switch and generate heat, but in the experiment, this inverter does not operate and the heat of the inverter was replaced by a cartridge heater. Therefore, the top part of the inverter was removed by milling, leaving only the baseplate, which is a pin-fin type heat sink made of copper, as shown in the figure 3.2. In addition, considering that the actual inverter is divided into three zones to generate heat in each zone, three brass blocks were produced as conductors for generating heat. Three brass blocks receive heat

from the cartridge heaters and serve to transfer it to the heat sink in the form of conduction. The brass block has 5 circular holes for inserting cartridge heaters and 2 small holes for inserting thermometers. After leaving only pin-fin type heat sink that are part of the existing inverter module, and after milling everything, three brass blocks are placed above the heat sink. Above them, heat insulating material made of ‘Bakelite’ is placed as shown in the figure 3.3.

Fig 3.1 IGBT module (Model: FS900R08A2P2_B31, Infineon)

Fig 3.2 Base plate (Pin-fin type heat sink)

Fig 3.3 Brass blocks, insulating material, and base plate

The heating value of 220 W can be generated per cartridge heater. Since five cartridge heaters can be installed for each brass block, and three brass blocks are placed on the pin-fin type heat sink, so this heating module can generate heat up to 3.3 kW as shown in the figure 3.4. It was assembled using thermal grease so that heat from the cartridge heaters conducts well to the brass block as shown in the figure 3.5. At the bottom part of heating module, a flow channel was created so that water and HFE-7100, which are working fluids for these experiments, could pass through the pin-fin type heat sink as shown in the figure 3.6. In particular, window made of polycarbonate was used to observe the point where bubbles are formed due to the boiling of HFE-7100.

In this experiment, the heating module that generates high heat is cooled by single-phase water and two-phase cooling method using HFE-7100 and the performance of the two cooling methods is compared by measuring the internal temperature of the heating module. Schematic and photo are shown in figure 3.7 and 3.8. Of the 12 thermometer installation points, six points were selected and marked at the figures. Also, in order to eliminate contact heat resistance, the heating module was strongly compressed through six vices.

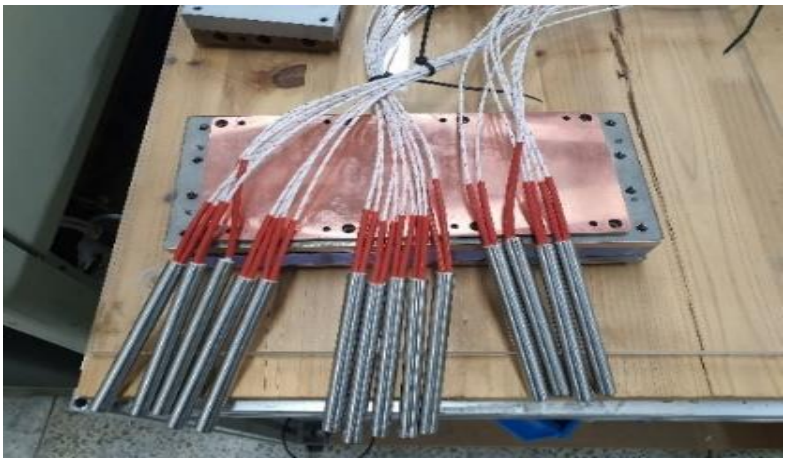

Fig. 3.4 Cartridge heater (220W/1ea, total 3.3kW/15ea)

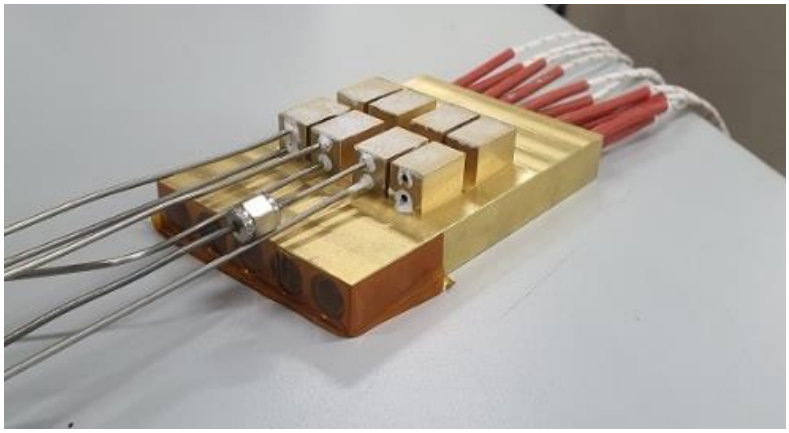

Fig. 3.5 Brass block & Cartridge heater assembly

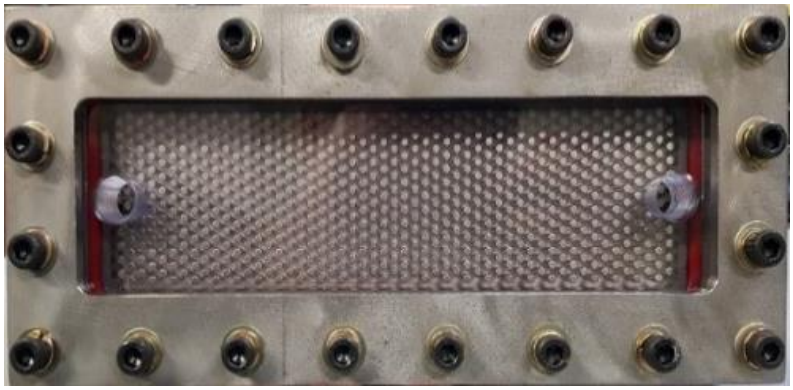

Fig 3.6 Flow channel

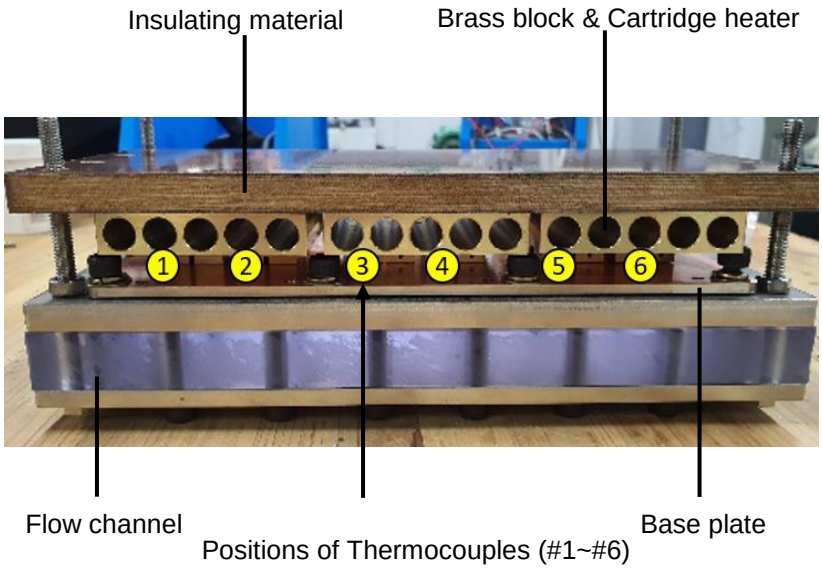

Fig 3.7. Photo of heating module

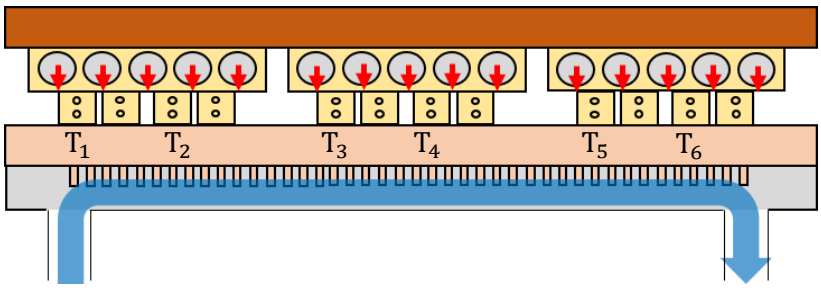

Fig 3.8. Schematic of heating module

Schematic and photo of heating module cooling system are shown in the figure 3.9 and 3.10. All system components are designed to create the same conditions as the environment inside the electric vehicle. Chiller and preheaters are installed to control and set the inlet temperature of working fluid entering the heating module. Mass flow meter control the flow rate of working fluid. Power consumption of the pump heat generation of heating module were measured through power meter, and the power supplied from the power supply to the cartridge heaters was controlled by 3 thyristors. A total of 12 thermometers at six points were installed in three brass blocks to measure the temperature inside the heating module. The differential pressure between the inlet and the outlet of the heating module was measured to determine how much pressure drop occurred as the fluid passed through the pin-fin type heat sink, which affect the pump power consumption. In addition, a pressure gauge was installed at the pump outlet to measure the maximum pressure of the entire system during the experiments.

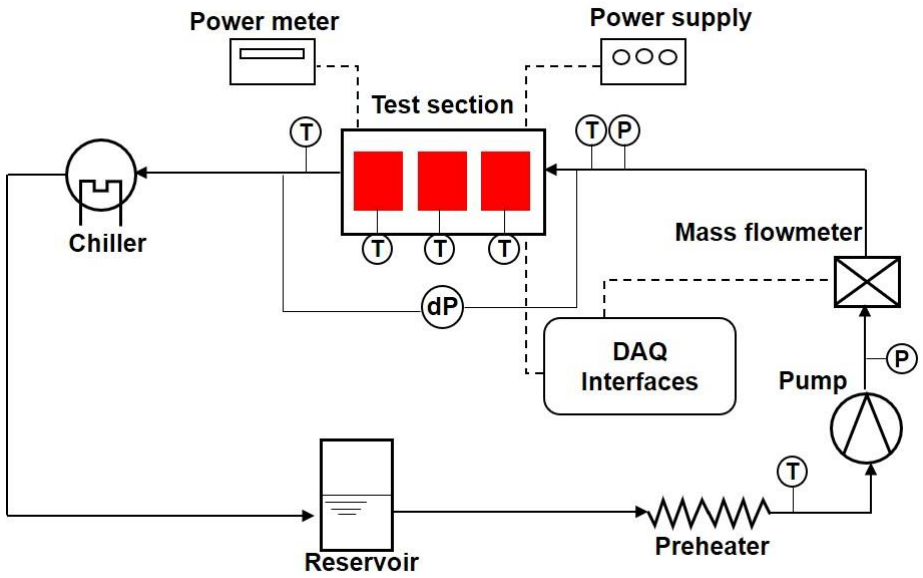

Fig 3.9. Schematic of heating module cooling system

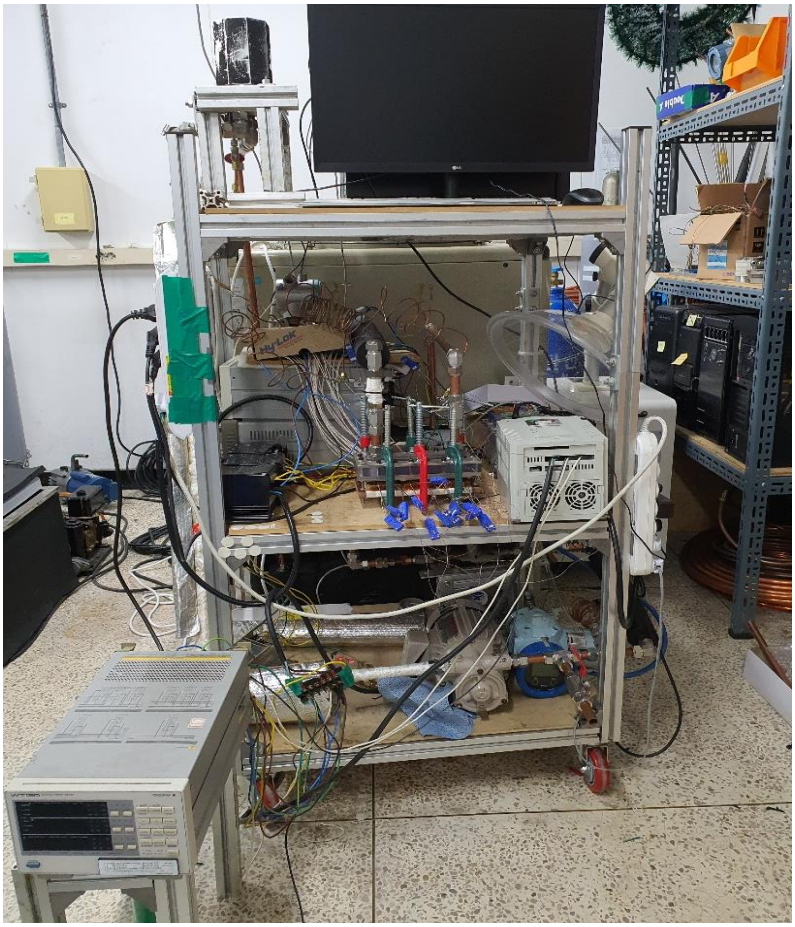

Fig 3.10. Photo of heating module cooling system

3.2 Experimental method

3.2.1 Measurement target

To compare the performance of each cooling experiment using water and HFE-7100, six positions were selected inside the heating module, and the temperature at each position was measured using thermometers installed. Thermometers were inserted into a 1.6 mm diameter holes in each brass block and the thermometer tip was treated by thermal grease for accurate temperature measurement. By measuring the temperature at six points, the average temperature and temperature distribution (uniformity) of the base plate (corresponding to IGBT junction temperature in actual inverter) are derived.

As measurement target, we choose average temperature, maximum temperature difference and standard deviation of temperature at 6 positions. The average temperature represents the operating temperature of the inverter, and standard deviation of temperatures represents the temperature uniformity. The temperature of each position is the surface temperature of baseplate and obtained by extrapolating the measured values of the temperature at two points of the brass block.

3.2.2 Experimental condition

We chose the refrigerant considering boiling temperature, environmental properties and electric resistance. Table 3.1 shows properties of water and HFE-

7100. In general, the coolant in the electric vehicles operates at a temperature of from 50℃ to 60℃. In order to induce phase change under these temperature conditions, a refrigerant which boils at a temperature slightly higher than the temperature inside the electric vehicle was required. Therefore, HFE-7100 with a boiling point of 61℃ at 1atm was selected. Also, ODP (Ozone Depletion Potential) and GWB (Global Warming Potential) of HFE-7100 is 0 and 320 respectively, which are significantly lower than those of the refrigerant $CFCl_3$, whose ODP is 1, or R-22, whose GWP is 1760. In addition, in order to cool the power electronic system, the lower the electrical conductivity, the better the safety, and the dielectric property of HFE-7100 is suitable for use in cooling electronic equipment. From these properties, HFE-7100 is considered appropriate refrigerant in power electronics system.

Before proceeding with this experiment, validation test was conducted. Figure 3.11 shows the results of the energy balance between supplied heat transfer rate measured by power meter and heat absorbed by water single-phase flow calculated based on temperature difference of inlet and outlet flow. Since the amount of heat supplied in the form of electric energy and the amount of heat absorbed by water matched with in an error range of 10%, it was confirmed that the energy balance was maintained well.

Figure 3.12 shows the results of heat transfer rate uniformity test, which compares the heat measured by the power meter and the heat calculated by measured temperature and thermal conductivity of brass block. This experiment was conducted to confirm that three thyristors supply the same amount of electrical energy to cartridge heaters installed on three brass blocks,

respectively. Heating value of each block was changed from 20 W to 40 W, and it was confirmed that three brass blocks generated same amount of heat within an error range of 10%, which satisfied energy balance validation.

Table 3.1 Material properties of water and HFE-7100

Properties	Water	HFE-7100
Boiling point at 1atm (℃)	100	61
Latent heat (J/kg-K)	2257	112
Liquid density (kg/m^3)	1000	1510
Liquid specific heat (J/kg-K)	4187	1183
ODP	-	0
GWP	-	320

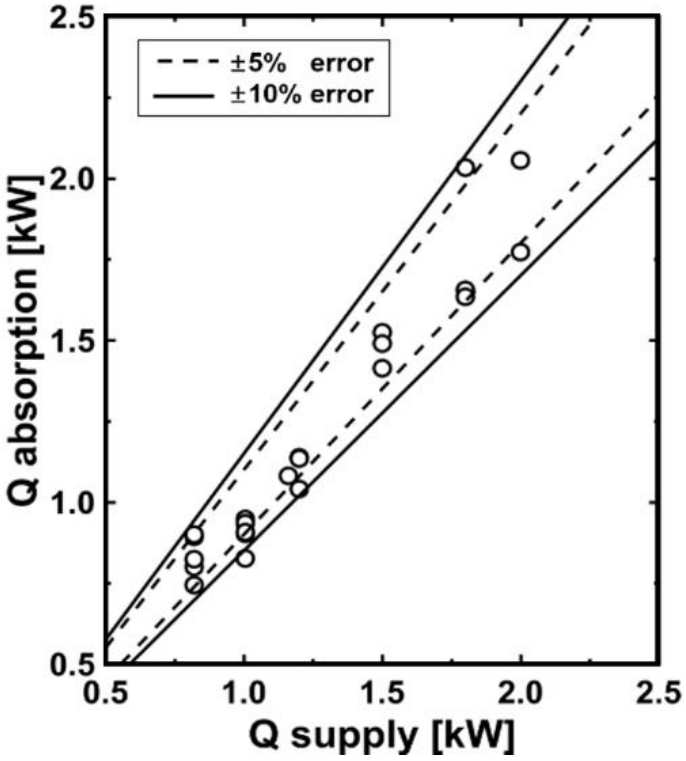

Figure 3.11 Energy balance in heating module cooling system.
(Comparison with supplied heat and absorbed heat by water)

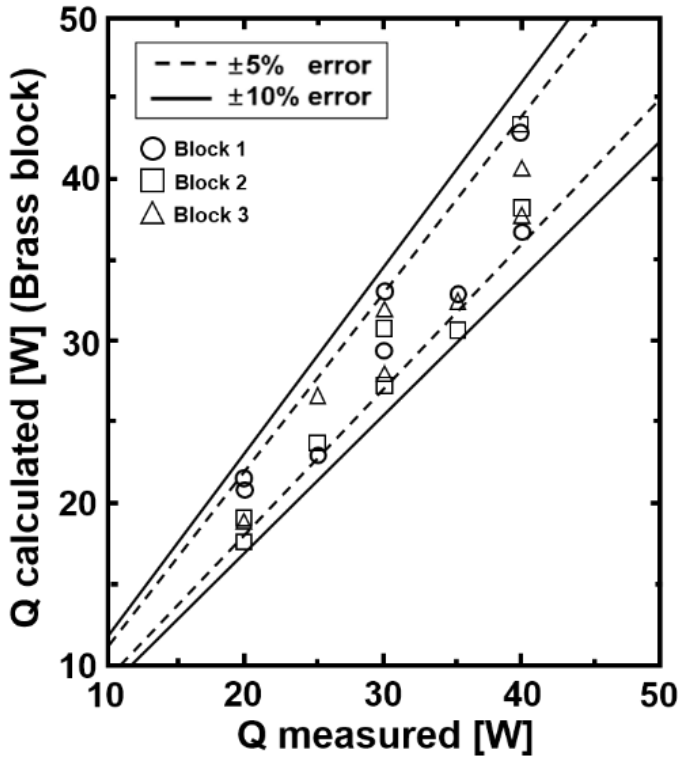

Figure 3.12 Heat transfer rates uniformity and energy balance of three brass blocks with measured values.

3.2.3 Experimental cases

The experimental cases were classified into the volumetric flow rate of working fluid and heat generated inside the heating module. In this experiment, as shown in the table 3.2 and 3.3, three experimental parameters are considered; inlet temperature, heat generation, and volumetric flow rate of working fluid. We conducted heating module cooling experiments in 18 cases of water and 21 cases in HFE-7100. Considering that the boiling point of HFE-7100 at 1atm is 61℃, the inlet temperature of the two working fluids was fixed at 46℃ ~ 48℃ which is controlled by preheater and chiller. This is due to the fact that the coolant temperature inside the electric vehicle is around 50℃. The working fluid that has passed through the heating module is cooled to about 30 ℃ by a chiller and then heated again to 46℃ ~ 48℃ by a preheater. The maximum power of the preheater is 1600 W, and it wraps the copper pipe through which the fluid flows and heats it.

In every experimental case, volumetric flow rate of water was increased from 2 LPM to 5 LPM with step size 1 LPM, and that of HFE-7100 was increased from 1 LPM to 4 LPM with step size 0.5 LPM. In the case of the refrigerant, the step size of the flow rate was set smaller than the step size of water because the cooling performance of the heat sink is significantly different due to the difference in the small flow rate. in addition, when the flow rate of the refrigerant becomes too large, no matter how large the amount of heat is generated, boiling does not occur inside the heating module, so the maximum flow rate was set to 4 LPM.

In order to generate more heat than values derived from the numerical model, which is around 1 kW range, the heat generation was changed from a minimum of 1.2 kW to 1.5 kW, 1.8 kW, 2.0 kW and 2.4 kW. This is because the output of the motor will increase as the size or weight of the electric vehicle increases, and the heat generation of the inverter will increase accordingly. The currently used pin-fin type heat sink can manage 1 kW level of heat, so in the experiments, we generate heat of 1.2 kW or more to show the effect of refrigerant two-phase cooling under extreme conditions. Also, since the maximum operating temperature of the inverter is 150℃, an experiment should be devised so that the temperature of the heating module does not exceed 150℃. That is, since the heat generation of the cartridge heaters cannot be increased infinitely, the maximum heat generation of the cartridge heaters was primarily set to 2.4 kW.

Table 3.2 Experimental cases of water single-phase cooling

Coolant flow rate	1.2 kW	1.5 kW	1.8 kW	2.0 kW
(LPM, g/s)	Inlet T 46~48°C			
2 (33.3)	W_1.2_2	W_1.5_2	W_1.8_2	-
3 (50.0)	W_1.2_3	W_1.5_3	W_1.8_3	-
4 (66.7)	W_1.2_4	W_1.5_4	W_1.8_4	W_2.0_4
5 (83.3)	W_1.2_5	W_1.5_5	W_1.8_5	W_2.0_5

Table 3.3 Experimental cases of HFE-7100 two-phase cooling

Coolant flow rate	1.2 kW	1.5 kW	1.8 kW	2.0 kW	2.4 kW
(LPM, g/s)	Inlet T 46~48°C				
1.0 (23.5)	R_1.2_1.0	R_1.5_1.0	-	-	-
1.5 (35.4)	R_1.2_1.5	R_1.5_1.5	-	-	-
2.0 (49.3)	R_1.2_2.0	R_1.5_2.0	-	-	-
2.5 (61.6)	R_1.2_2.5	R_1.5_2.5	R_1.8_2.5	R_2.0_2.5	-
3.0 (72.6)	-	R_1.5_3.0	R_1.8_3.0	R_2.0_3.0	-
3.5 (84.7)	-	-	R_1.8_3.5	R_2.0_3.5	R_2.4_3.5
4.0 (96.8)	-	-	R_1.8_4.0	R_2.0_4.0	R_2.4_4.0

3.3 Experimental results

3.3.1 Experimental results of water single-phase cooling and HFE-7100 two-phase cooling

Fig 3.13 ~ 3.16 shows the peak temperature comparison of 6 positions inside the heating module by water single-phase cooling and HFE-7100 two-phase cooling. Figures show the results of experiments when heat generation of 1.2 kW, 1.5 kW, 1.8 kW and 2.0 kW were applied respectively. Black markers with solid lines are the results of refrigerant, and hollow marker with dash lines are the results of water experiments. In all cases, it was confirmed that the peak temperature of each position decreased as the flow rate of the working fluid increased. Also, it can be seen that the temperature difference between point 1 and point 6 increases as the heating value of the cartridge heaters increases. When the heat generation of 1.2 kW (Figure 3.13), the HFE-7100 showed cooling performance comparable to that of water at smaller volumetric flow rates. This indicates that the pin-fin type heat sink used in the experiment can be thermally managed by the water single-phase cooling method even at a heating amount of 1.2 kW, which is a heat amount that can be generated in an actual driving situation. When the heat generation is 1.5 kW or more (Figure 3.14 ~ 3.16), which is larger than the heat generated in actual driving situation, it was confirmed that HFE-7100 two-phase cooling showed lower temperature in 6 positions and temperature difference between the highest and lowest temperatures inside the heating module was smaller than water single-phase

cooling. As the amount of heat increased, the difference in cooling performance between the water single-phase cooling method and the HFE-7100 two-phase cooling method became apparent. This is because the larger the amount of heat generated in the heating module, the more actively the boiling of HFE-7100 occurs. Therefore, if the heat generation of cartridge heaters is increased and the flow rate of HFE-7100 is increased to a certain level that the latent heat of the HFE-7100 can sufficiently absorb the heat amount of the heater, the cooling effect of the inverter will be maximized.

Especially, it was confirmed that when the heat generation exceeds 2.0 kW, the temperature of the heating module could not be maintained below 150℃ (Maximum operating temperature of inverter) no matter how much the water flow rate was increased. This clearly shows the limitations of the water single-phase cooling method and in other words, in the high-powered electric vehicles of the future, the use of water single-phase cooling method is no longer a limitation. On the other hand, when the heat generation is 2.4 kW, HFE-7100 two-phase cooling was able to keep the inverter temperature below 150 ℃. Also, in all experiments, HFE-7100 two-phase cooling method showed higher cooling performance even though a smaller flow rate was applied compared to the water experiment. The small flow rate has the effect of reducing the power consumption of the pump. That is, the HFE-7100 two-phase cooling has greater inverter cooling performance using less pump consumption power.

From all the experimental results, it was confirmed that the temperature in position 2 is higher than the temperature in position 3. This is the effect of a confined liquid impingement jet. When the fluid enters the inlet of the heating

module, it falls vertically and hits the base plate, and flows toward the outlet. There are many theories and experimental results which prove that the ratio of the height of the flow channel and the diameter of the inlet flow path and is smaller than 2, the Nusselt number locally has a second maximum value which is called ‘Secondary peak’ [16] as shown in the figure 3.17. It is believed that the rapid increase in turbulence entails transition process from the flow of accelerated stagnation zone to deceleration wall jet. In this experiment, height of the flow channel is 1cm and the diameter of the inlet flow path is 2.54cm ($H/D < 2$). It is the condition to be able to have the secondary peak and this can explain why the temperature of point 2 is higher than that of point 3 in all experimental cases.

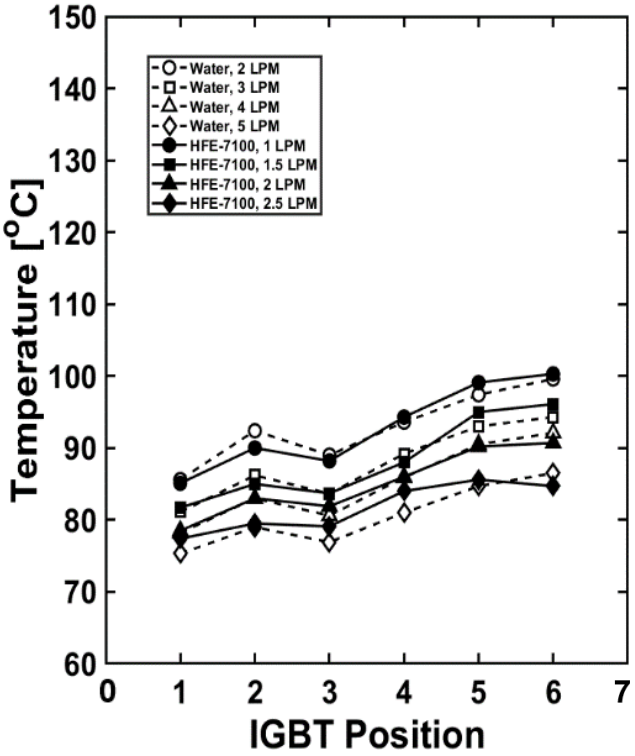

Fig. 3.13 Peak temperature comparison of 6 positions inside the heating module by HFE-7100 two-phase cooling and water single-phase cooling. (Heat generation 1.2 kW)

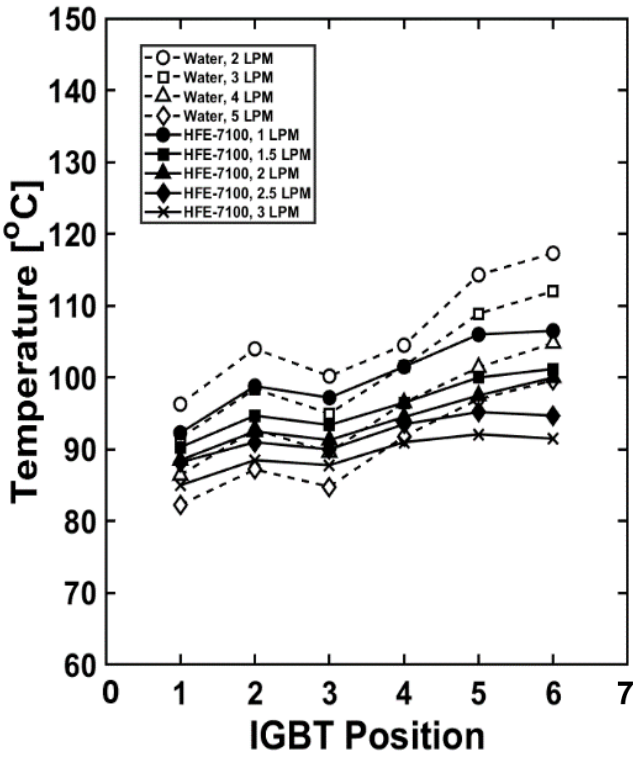

Fig. 3.14 Peak temperature comparison of 6 positions inside the heating module by HFE-7100 two-phase cooling and water single-phase cooling. (Heat generation 1.5 kW)

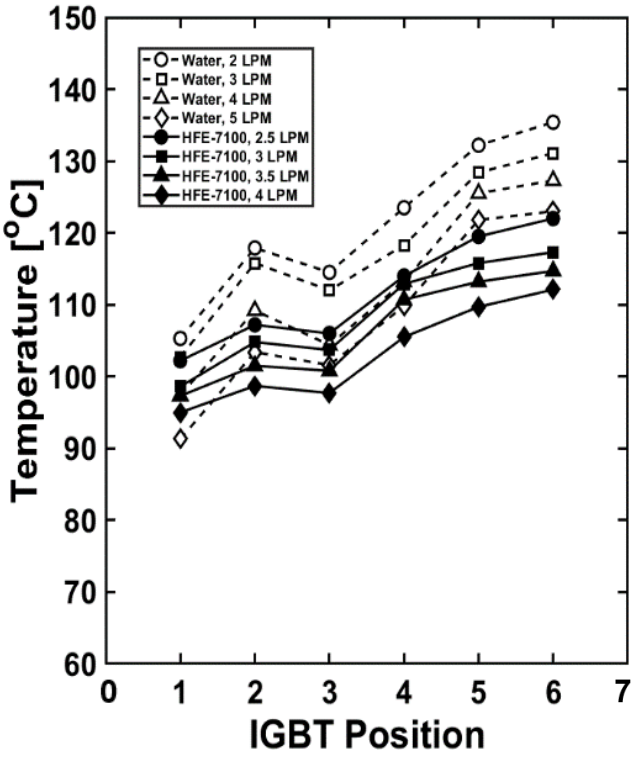

Fig. 3.15 Peak temperature comparison of 6 positions inside the heating module by HFE-7100 two-phase cooling and water single-phase cooling. (Heat generation 1.8 kW)

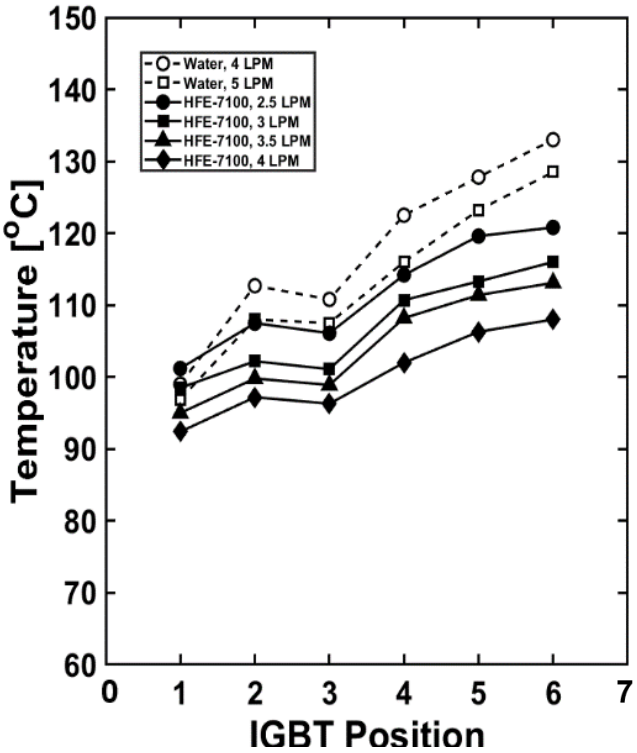

Fig. 3.16 Peak temperature comparison of 6 positions inside the heating module by HFE-7100 two-phase cooling and water single-phase cooling. (Heat generation 2.0 kW)

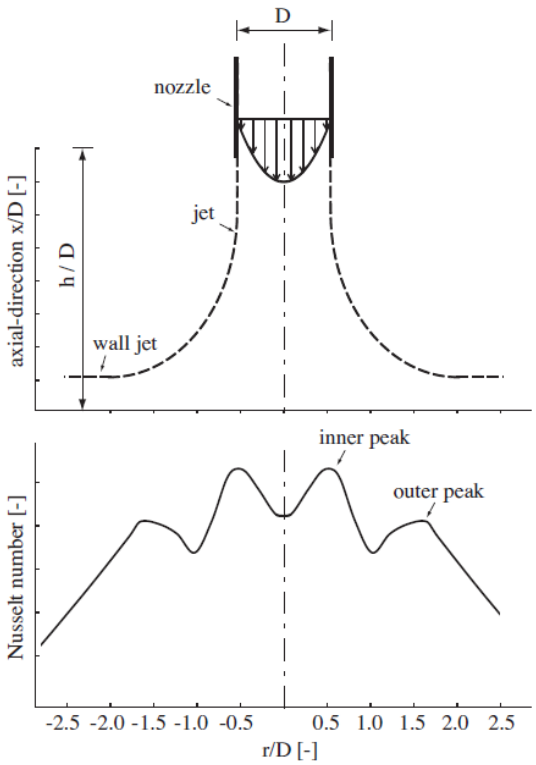

Fig 3.17 Characteristics of an impinging jet: flow field (top) and heat transfer distribution (bottom). [16]

3.3.2 Discussion

3.3.2.1 Average temperature and maximum temperature difference

Figure 3.18 ~ 3.21 show the average temperature and temperature ranges from lowest to highest temperatures. In the figures, red circles are the average temperature of 6 positions as a result of the water single-phase cooling experiment, and blue triangles are the results of the HFE-7100 two-phase cooling experiment. Also, Temperature ranges from lowest to highest temperatures are indicated in the form of error bars according to the volumetric flow rate of working fluid. The long error bar means that the difference between the lowest and highest temperature inside the inverter is large, that is, the temperature inside the heating module is not uniform. In all experiments, it can be seen that the smaller the flow rate and the larger the amount of heat generated inside the heating module, the longer the error bar, and it means bad temperature uniformity.

As heat generation increases, the effect of lowering average temperature of the heating module with two-phase cooling is significantly better than single-phase cooling. This is because, as mentioned above, as the amount of heat increases, the boiling of the refrigerant may occur actively, and the utilization of latent heat becomes easier. As a results of two-phase cooling experiments, the average temperature inside the heating module was lower than the single-phase cooling in all the experimental cases and difference is by up to 13℃. In addition, in all experiment results, the maximum temperature difference inside

the heating module was found to be lower in the two-phase cooling experiments and its value is up to 16℃. When the temperature difference decreases, the physical deformation caused by the temperature difference also decreases, which significantly increases the life span and reliability of the product. This mean is that by just changing the working fluid used for cooling, we can reduce the potential cost savings. In particular, in the case of heat generation of 2.0 kW, it was possible to maintain the temperature of the heating module below the 150℃ only when the flow rate of water was 4 LPM or more. On the other hand, in the case of HFE-7100, it was possible to sufficiently cool even if only a flow rate of 2.5 LPM or more was flowed, and the internal temperature difference and average temperature were also significantly low.

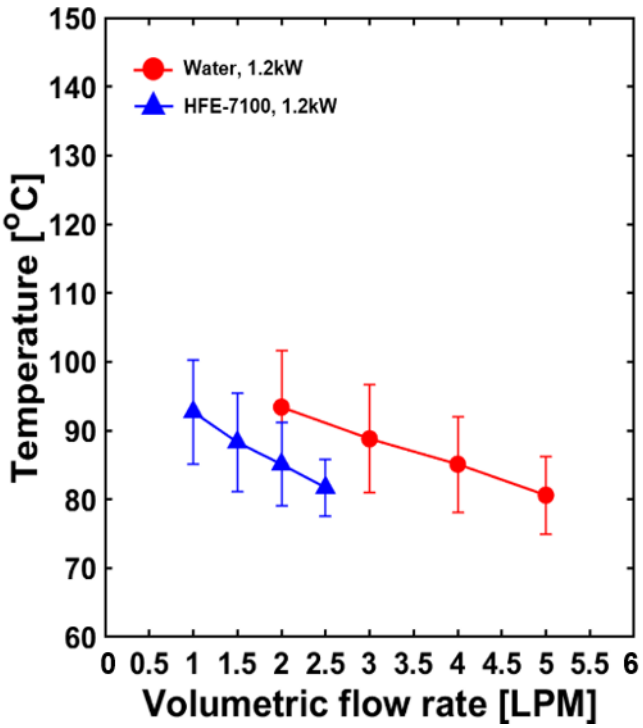

Fig. 3.18 Average temperature and temperature ranges from lowest to highest temperatures of the 6 positions inside of the heating module. (Heat generation: 1.2 kW)

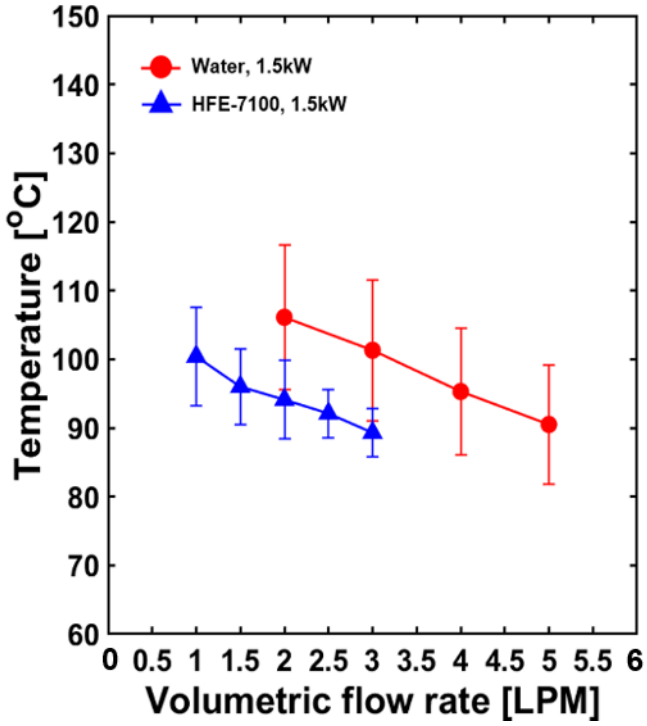

Fig. 3.19 Average temperature and temperature ranges from lowest to highest temperatures of the 6 positions inside of the heating module. (Heat generation: 1.5 kW)

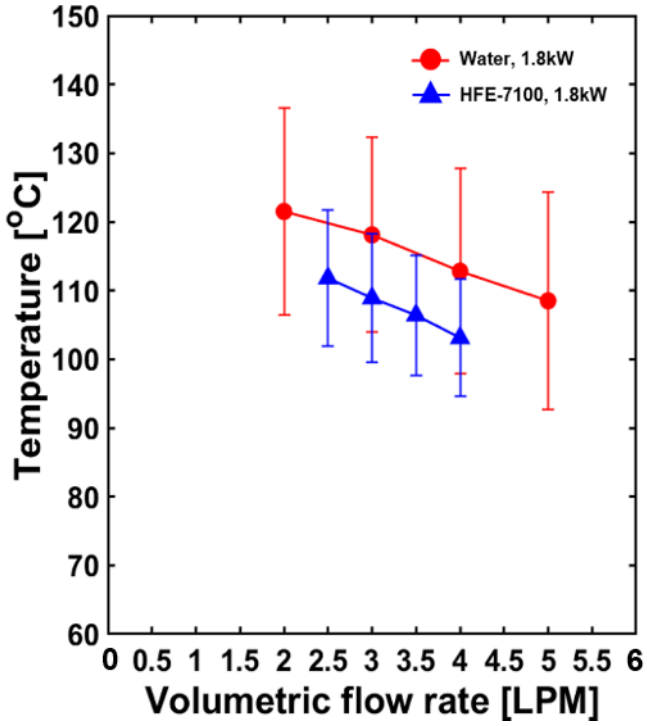

Fig. 3.20 Average temperature and temperature ranges from lowest to highest temperatures of the 6 positions inside of the heating module. (Heat generation: 1.8 kW)

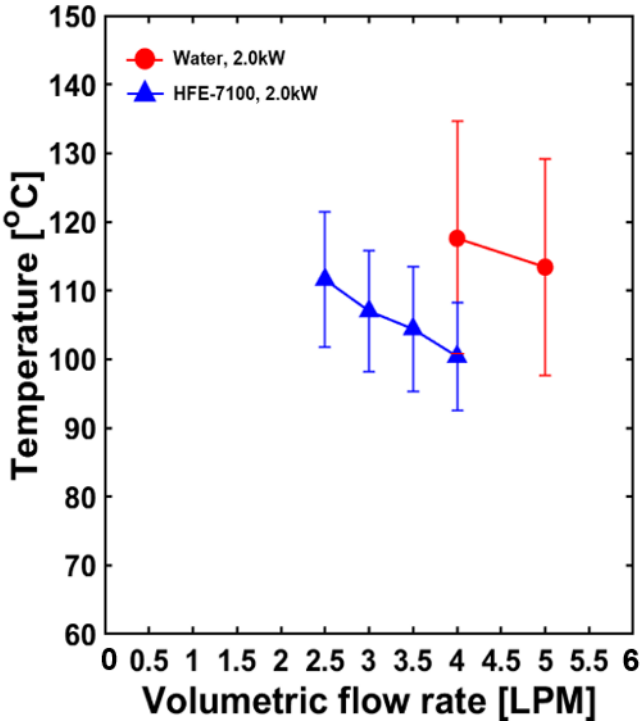

Fig. 3.21 Average temperature and temperature ranges from lowest to highest temperatures of the 6 positions inside of the heating module. (Heat generation: 2.0 kW)

3.3.2.2 Temperature uniformity

As described above, temperature uniformity inside the inverter is an important factor because it greatly affects the life span and reliability of the product. In this study, temperature uniformity is validated by calculating standard deviation of temperature at 6 positions. In terms of temperature uniformity, it was found that the cooling performance of HFE-7100 two-phase cooling was much improved than that of water single-phase cooling considering standard deviation of inside temperature the heating module in each experimental result despite the lower volumetric flow rate.

Except for the two cases at 1.2 kW, the two-phase cooling experiments showed lower temperature standard deviations in all experimental cases, which mean is better temperature uniformity. The exceptional two cases of 1.2 kW also showed a small difference of temperature standard deviation because the volumetric flow rate of the HFE-7100 was smaller than that of water. Assuming that the flow rate was the same with water, the temperature standard deviation in the HFE-7100 two-phase cooling experiment was expected to be much smaller than water single-phase cooling experiment.

According to the volumetric flow rate and heat generation, every experimental case was classified into 14 cases (Two cases of two-phase cooling experiment results when 2.4 kW of heat was applied were omitted because they could not be compared with the results of water-cooling experiments). Each case consists of data from one experiment of water and that of refrigerant, and every case summarized in table 3.4. The standard deviation of temperature for

each experiment results is shown in figures 3.22 ~ 3.25. As can be seen from the figures, the boiling cooling of the refrigerant showed better temperature uniformity through a lower flow rate than that of water cooling. Especially, it was shown that when the same amount of heat is applied, the differences in temperature uniformity between the two working fluids increases as the volumetric flow rate of the fluid increases.

Table 3.4 Classification of experiments for comparison of standard deviations of temperature of heating module

Case	Heat generation	Water (LPM)	HFE-7100 (LPM)
1	1.2 kW	2	1.0
2		3	1.5
3		4	2.0
4		5	2.5
5	1.5 kW	2	1.0
6		3	1.5
7		4	2.0
8		5	2.5
9	1.8 kW	2	2.5
10		3	3.0
11		4	3.5
12		5	4.0
13	2.0 kW	4	3.5
14		5	4.0

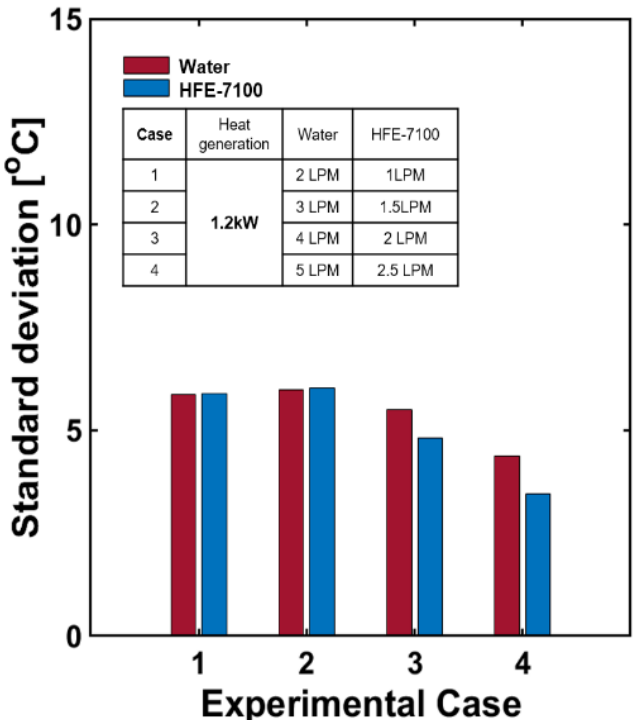

Fig. 3.22 Standard deviation of temperature inside the heating module (Experimental case: 1~4)

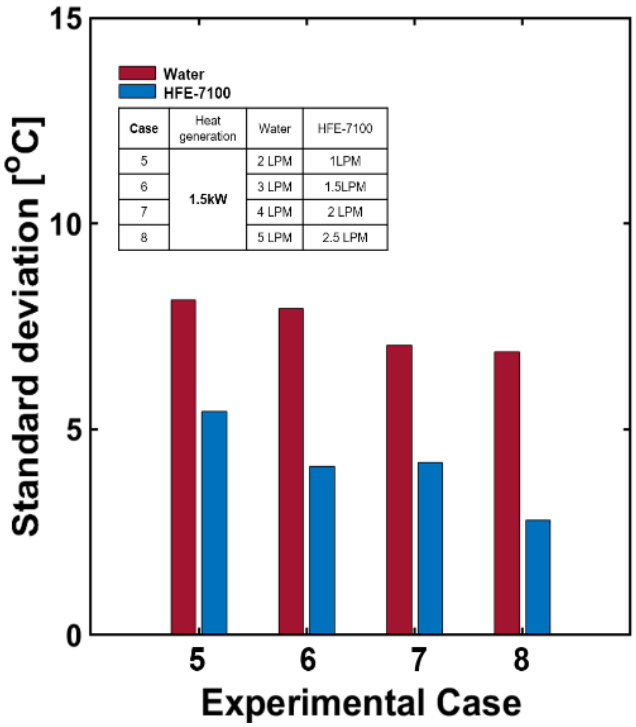

Fig. 3.23 Standard deviation of temperature inside the heating module (Experimental case: 5~8)

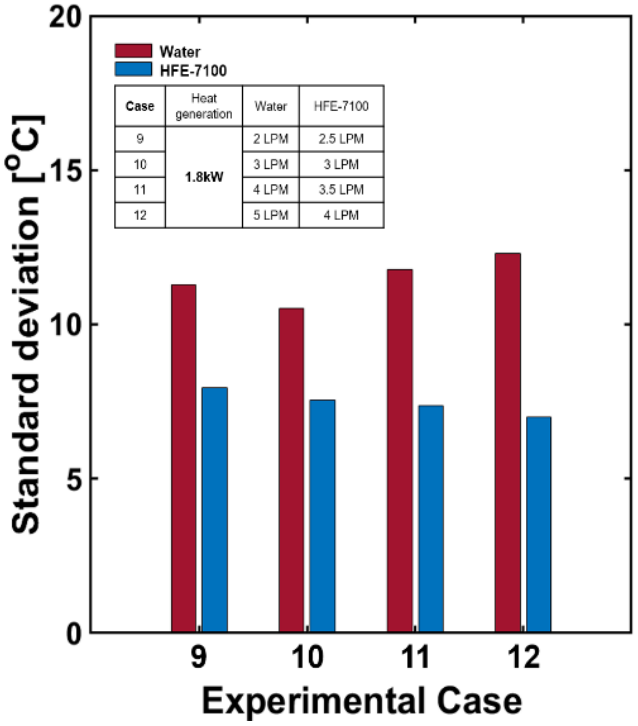

Fig. 3.24 Standard deviation of temperature inside the heating module (Experimental case: 9~12)

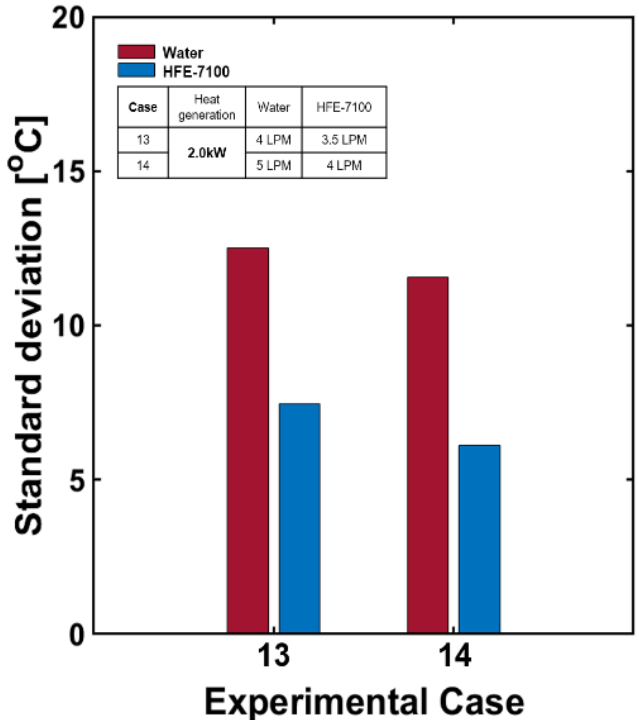

Fig. 3.25 Standard deviation of temperature inside the heating module (Experimental case: 13~14)

4. Conclusion

As a result of the experiment, the water single-phase cooling experiment showed the limitation of heat dissipation capacity of about 2 kW. On the other hand, the HFE-7100 two-phase cooling experiment showed heat dissipation capacity of over 2.4 kW even at a smaller volumetric flow rate.

Also, The HFE-7100 two-phase cooling experiment showed lower average temperature and better temperature uniformity within the entire IGBT module than that of water single-phase cooling. Uniform temperature distribution is a highly desired merit for high heat flux cooling technologies since it improves device reliability and reduces the severity of fatigue mechanism.

As a result of analyzing all the experimental results, using the two-phase cooling method, it is expected that the temperature of the inverter can be maintained under the allowable operating temperature (120°C) even at a higher heat generation. As shown in the figure 4.1, two-phase cooling method can reduce operating temperature of inverter through less power consumption of pump. In other words, it means that higher cooling performance make power electronics system enable to output high power densities while maintaining acceptable device temperatures.

Finally, it can make potential cost reduction effect by achieving same power level with fewer devices and lighter weight package than conventional IGBT module by using refrigerant two-phase cooling method.

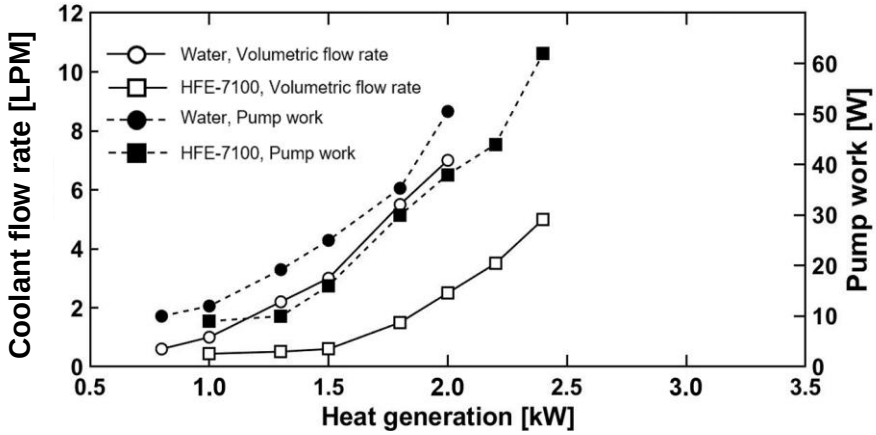

Fig 4.1 Minimum volumetric flow rate and pump work to maintain IGBT temperature under 120°C

References

[1] Ets.krx.co.kr, Price of certified emissions reduction from 2018 to 2020.

[2] L Meysenc, M. Jylhakallio, and P. Barbosa, “Power electronics Cooling Effectiveness Versus Thermal Inertia,” *IEEE Trans*. *Power Electron.,* vol 20, no. 3, pp.687-693, May 2005.

[3] USDA, Economic Research Service using data from the U.S. Environmental Protection Agency, April 2020: Inventory of U.S. Greenhouse Gas Emissions and Sinks: 1990-2018

[4] J. de Santiago, H. Bernhoff, B. Ekergard, S. Eriksson, S. Ferhatovic, R. Waters, and M. Leijon, “Electrical motor drivelines in commercial all-electric vehicles: A review,” *IEEE Trans. Veh. Technol.,* vol. 61, no. 2, pp. 475-484, Feb. 2012.

[5] M. J. Rau, E. M. Dede, and S. V. Garimella, “Local single- and two-phase heat transfer from an impinging cross-shaped jet,” *Int. J. Heat Mass Transfer.,* vol. 79, pp. 432-436, Aug. 2014.

[6] A. Bhunia, Q. Cai, and C. L. Chen, ”Liqiud impingement and phase change for high power density electronic cooling,” *Proceeding of the 41st AIAA Aerospace Sciences Meeting and Exhibit.*, Reno, NV, 2003.

[7] A. Bhunia and C. L. Chen, “Jet impingement cooling of an inverter module in the harsh environment of a hybrid vehicle,” *Proceeding of ASME Summer*

Heat Transfer Conference., San Francisco, CA, Paper No. HT2005-72574. Jul. 2005.

[8] P. R. Parida, S. V. Ekkad, and K. Ngo, "Impingement-based high performance cooling configurations for automotive power converters," *Int. J. Heat Mass Transfer*., vol. 55, pp. 834-847, Jan. 2012.

[9] I. Mudawar, D. Bharathan, K. Kelly, and S. Narumanchi, "Two-phase spray cooling of hybrid vehicle electronics," *IEEE Trans. Comp. Packag. Technol.,* vol. 32, no. 2, pp. 501-512, Jun. 2009.

[10] H. Bostanci, D. V. Ee, B. A. Saarloos, D. P. Rini, and L. C. Chow, "Thermal management of power inverter modules at high fluxes via two-phase spray cooling," *IEEE Trans. Compon. Packag. Manuf. Technol.,* vol. 2, pp. 1480-1485, Sept. 2012.

[11] B. L. Rowden, D. W. Trowler, and J. C. Balda, "Double-sided spray cooled bi-directional power conversion module," *in Proc. Electr. Ship Technol. Symp.,* Baltimore, MD, pp. 207-210, May 2009.

[12] J. Lee and I. Mudawar, "Two-phase flow in high-heat-flux micro-channel heat sink for refrigeration cooling applications, Part I: Pressure drop characteristics," *Int. J. Heat Mass Transfer*., vol. 48, pp. 928-940, 2005.

[13] J. Lee and I. Mudawar, “Two-phase flow in high-heat-flux micro-channel heat sink for refrigeration cooling applications, Part II: Heat transfer characteristics,” *Int. J. Heat Mass Transfer.*, vol. 48, pp. 928-940, 2005.

[14] P. Wang, P. McCluskey, and A. Bar-Cohen, “Two-phase liquid cooling for thermal management of IGBT power electronic module,” *J. Electron. Packag.,* vol. 135, 2013.

[15] C. Qian, A. M. gheitaghy, J. Fan, H. Tang, B. Sun, H. Ye, and G, Zhang, “Thermal management on IGBT power electronic devices and modules,” *IEEE Access.*, vol. 6, pp. 12 868-12 884, 2018.

[16] W. Rohlfs, H. D. Haustein, O. Garbrecht, and R. Kneer, “Insights into the local heat transfer of a submerged impinging jet: Influence of local flow acceleration and vortex-wall interaction,” *Int. J. Heat Mass Transfer.*, vol. 55, pp. 7728-7736, 2012.

[17] K. Kumar, M. Bertoluzzo, G. Buja, and F. Ortenzi, “Quantitative analysis of efficiency improvement of a propulsion drive by using sic devices: A case of study,” *Journal of Advances in Power Electronics.*, Article ID 9149472, pp. 1-10, 2017.

[18] N. Rao and D. Chamund, “Calculating power losses in an IGBT module,” *Application Note.*, AN6156-1, Sep. 2014.

[19] Y. Wang, X. Dai, G. Liu, Y. wu, D. Li, and S. Jones, “Integrated liquid

cooling automotive IGBT module for high temperatures coolant application," in *Proc. PCIM.,* Nuremberg, Germany, pp. 1197-1203, May 2015.

[20] J. Lee, S. Ki, D. Seo, J. Kim and Y. Nam, "Liquid cooling module incorporating a metal foam and fin hybrid structure for high power insulated gate bipolar transistors (IGBTs)," *Applied Thermal Engineering.*, vol. 173, June 2020.

[21] L. Meysenc, M. Jylhakallio, and P. Barbosa, "Power electronics cooling effectiveness versus thermal inertia," *IEEE Trans. Power Electron.*, vol. 20, pp. 687–693, May 2005.

[22] Z. Xu, M. Li, F. Wang, and Z. Liang, "Investigation of Si IGBT operation at 200 ◦C for traction application," *IEEE Trans, Power Electron.,* vol. 28, no. 5, pp. 2604–2615, May 2013.

[23] J. B. Campbell, L. M. Tolbert, C. W. Ayers, B. Ozpineci, and K. T. Lowe, "Two-phase cooling method using the R134a refrigerant to cool power electronic devices," *IEEE Trans. Ind. Appl.,* vol. 43, no. 3, pp. 648-656, May 2007.

[24] W. Mazgaj, B. Rozegna, and Z. Szular, "Switching losses in three-phase voltage source inverters," *Czasopismo Techniczne*, vol. 13, pp. 47–60, 2016.

[25] Y. Wang, S. Jones, A. Dai, and G. Liu, “Reliability enhancement by integrated liquid cooling in power IGBT modules for hybrid and electric vehicles,” *Microelectron. Rel.*, vol. 54, no. 9–10, pp. 1911–1915, Sep./Oct. 2014.

[26] W. A. Khan, J. R. Culham, and M. M. Yovanovich, “Modeling of cylindrical pin-fin heat sinks for electronic packaging,” *IEEE Trans. Compon. Packag. Tech.*, vol. 31, no. 3, pp. 536-545, Sept. 2008.

[27] A. Christmann, M. Thoben, and K. Mainka, “Reliability of power modules in hybrid vehicles,” in *Proc. Power Electron. Intell. Motion Power Quality Conf.*, pp. 359-366, 2009.

[28] S. G. Kandlikar, “A general correlation for saturated two-phase flow boiling heat transfer inside horizontal and vertical tubes,” *J. Heat Transfer.,* Feb. 1990.

[29] X. Lu, Y. Wu, L, Zhou, G. Su, S. Qiu, and H. Zhang, “Theoretical investigations on two-phase flow instability in parallel channels under axial non-uniform heating,” *Annals of Nuclear Energy.,* vol. 63, pp. 75-82, Jan. 2014.

[30] International Energy Agency, “Technology roadmap: Electric and plug-in hybrid electric vehicles,” Jun. 2009.

[31] J. Lee, S. Ki, and Y. Nam, “Compact liquid cooling system incorporating fin and porous layer hybrid structures for high power IGBTs,” *IEEE. ITherm.,* 2019

[32] Y. C. Sa, S. M. You, and J. S. Lee, “Pressure drop of two-phase flow in helically coiled tubes,” SAREK, 1999.

[33] Sun Jin Kim, “Study on the thermal management of motor in electric vehicle using flow boiling heat transfer in curved channel,” Seoul National University, 2019.

[34] H. Song and G. Lim, “Hybrid electric propulsion system configuration for analyzing heat generation characteristic of power conversion device,” KIEE, pp. 1145-1146, 2019.

[35] S. Ki, J. Lee, S. Ryu, and Y. Nam, “Compact liquid cooling system for high power IGBT modules in EV/HEV Applications," *Int. Heat Transf. Conf.,* pp. 3833-3839, 2018.

[36] J. R. Rybicki and I. Mudawar, “Single-phase and two-phase cooling characteristics of upward-facing and downward-facing sprays,” *Int. J. Heat Mass Transfer.,* vol. 49, pp. 5-16, Jan. 2006.

[37] L. Lin and R. Ponnappan, “Heat transfer characteristics of spray cooling in a closed loop,” *Int. J. Heat Mass Transfer.,* vol. 46, no. 20, pp. 3737-3746, Sept. 2003.

[38] J. Seo and M. Lee, “Numerical analysis on cooling characteristic of the heat sink for amplifier,” *Journal of the Korea Academia-Industrial cooperation Society.,* vol. 16, no. 2, pp. 947-951, 2015.

[39] J. B. Marcinichen, J. R. Thome, and B. Michel, “Cooling of microprocessors with micro-evaporation: A novel two-phase cooling cycle,” *Int. J. Refrigeration.,* vol. 33, no. 7, pp. 1264-1276, Nov. 2010.

[40] M. J. Rau and S. V. Garimella, “Confined jet impingement with boiling on a variety of enhanced surfaces,” *J. Heat Transfer.*, vol 136, no. 10, p. 101503, Jul. 2014.

[41] M. J. Rau, “Turbulent liquid-vapor flow interactions and heat transfer in confined jet impingement boiling,” Purdue University, 2016.

[42] M. J. Rau and S. V. Garimella, “Local two-phase heat transfer from arrays of confined and submerged impinging jets,” *Int. J. Heat Mass Transfer.,* vol. 67, pp. 487-498, Dec. 2013.

[43] H. Park, J. Ha, G. Lee, and J. Jung, “Flux weakening control based on stator flux linkage with robustness against voltage fluctuation in high speed region of IPMSM for automotive,” J*ournal of Institute of Control, Robotics and Systems.,* vol. 23, no. 12, pp. 1027-1035, 2017.

[44] K. Li, and Y Wang, “Maximum Torque per Ampere (MTPA) control for IPMSM drives using signal injection and an MTPA control law,” *IEEE*

Trans. Ind. Informat., vol. 15, no. 10, pp. 5588-5598, Oct. 2019.

[45] Multisim Education Edition Help 372062L-01 – National Instruments, 2015.

[46] W. Yu, D. M. France, M.W. Wambsganss, and J. R. Hull, "Two-phase pressure drop, boiling heat transfer, and critical heat flux to water in a small-diameter horizontal tube," *Int. J. Multiphase Flow.,* vol. 28, no. 6, pp. 927-941, 2002.

[47] W. Qu and I. Mudawar, "Flow boiling heat transfer in two-phase micro-channel heat sinks-I. Experimental investigation and assessment of correlation methods," *Int. J. Heat Mass Transfer.,* vol. 46, no. 15, pp. 2755-2771, Jul. 2003.

국 문 초 록

전기자동차의 전력전자 시스템의 고출력화 및 소형화의 필요성이 대두되고 있으며, 이에따라 전력전자시스템의 열 관리는 전기자동차 산업의 확장과 함께 중요한 이슈가 되고 있다.

본 연구에서는 전기자동차의 전력전자 시스템을 구성하는 요소 중 하나인 인버터를 효과적으로 냉각하는 방법으로써 HFE-7100 냉매를 이용한 2 상 비등 냉각방식을 제시하여, 인버터 작동온도 및 내부온도 편차를 줄일 수 있음을 보이는 연구를 진행하였다.

또한, 인버터의 발열량을 예측하기 위해 시뮬레이션 연구를 진행하였다. 여러 가지 주행조건에서 필요로 하는 모터의 전류를 다양한 제어방법을 통해 계산하였고, 최종적으로 자동차의 주행조건 별 인버터에서 발생하는 전도 열 손실, 스위칭 손실을 산출하는 모델을 제시하였다.

HFE-7100 냉매를 이용한 비등 냉각방식을 차량용 인버터에 적용하는 실험을 진행하였고, 그 결과를 기존에 사용하던 방식인 수냉식 냉각방식을 적용한 실험 결과와 비교하였다. 그 결과, 냉매 비등 냉각방식이 수냉식 냉각방식보다 더 적은 펌프 소모동력을 통해, 인버터가 더 낮은 평균온도 및 균일한 온도분포를 보임을 확인하였다.

전기자동차의 엔진역할을 하는 전력전자 시스템의 구성품 중 하나인 인버터를 효과적으로 냉각함으로써, 인버터의 작동온도를 낮추어 시스템 안정성을 높이고 내부의 온도 편차에 의한 물리적인

변형을 줄여 제품의 수명과 신뢰성을 향상시킬 수 있다. 또한 미래에 전력전자 시스템이 에너지의 고밀도화, 시스템의 소형화를 이루어 내고, 전력전자시스템 냉각에 대한 잠재적인 비용절감효과를 가져오기 위해서는 냉매를 이용한 비등 냉각방식이 적절한 해결책이 될 수 있음을 증명하였다.

주요어: 전기자동차, 전력전자시스템, 비등냉각, Pin-fin형 방열판, 열 관리, HFE-7100

학번: 2018-27952